ORIGINAL PAPER

J. Yao · K. Konstantinov · G. X. Wang · H. K. Liu

Electrochemical and magnetic characterization of LiFePO$_4$ and Li$_{0.95}$Mg$_{0.05}$FePO$_4$ cathode materials

Abstract A series of lithium iron phosphates was synthesized via the sol–gel route. Iron phosphides, which are electronic conductors, were formed when sintered at 850°C. Magnetic susceptibility measurements on the samples show antiferromagnetic behaviour with T_N=50±2 K for LiFePO$_4$ and Li$_{0.95}$Mg$_{0.05}$PO$_4$ sintered at temperatures below 850°C. The LiFePO$_4$ and Li$_{0.95}$Mg$_{0.05}$FePO4 cathodes show a stable electrochemical capacity in the range of 150–160 mA h/g on cycling. The cyclability deteriorates with increasing sample sintering temperature due to the increased crystal size and impurities.

Introduction

Lithium-ion batteries have become the dominant power sources for portable electronic devices because of their high energy density [1–4]. The current commercial lithium-ion batteries use LiCoO$_2$ as the cathode material, which limits the applications to small batteries due to the high cost and toxicity of Co. In the past decade, a number of new cathode materials such as layered structure of LiMnO$_2$ [5, 6], LiMn$_2$O$_4$ spinels [7, 8] and LiM$_x$Ni$_{1-x}$O$_2$ compounds [9, 10] have been developed as alternative cathode materials for lithium-ion batteries. However, none of them are in real industrial applications so far.

A group of lithium transition metal "polyanion" compounds incorporating polyanions XO$_4^{3-}$ (X=S, P, As, Mo) has been extensively investigated as new cathode

materials for lithium-ion batteries [11–15]. Among them, LiFePO$_4$ olivines have attracted particular interest because of the low cost and environmental friendliness of iron. LiFePO$_4$ has a lithium intercalation/de-intercalation potential of 3.4–3.5 V vs Li/Li$^+$ due to the tuning effect of the large polyanion [PO$_4$]$^{3+}$. LiFePO$_4$ is an ideal cathode material for large-scale lithium-ion batteries for electric vehicles (EVs) and stationary power storage. LiFePO$_4$ has an ordered olivine structure (space group *Pnma*), in which Li, Fe and P atoms occupy octahedral 4a, octahedral 4c and tetrahedral 4c sites, respectively. The oxygen atoms are arranged in a slightly distorted, hexagonal close-packed arrangement. The FeO$_6$ octahedra share common corners in the bc plane, and the LiO$_6$ octahedra form an edge-sharing chain in the *b*-direction. The separation of the FeO$_6$ octahedra by PO$_4$ polyanions significantly reduces the electrical conductivity of the material. This causes poor rate capacity and low utilization of Li in the LiFePO$_4$ host structure. Extensive investigations have been made to improve the performance of LiFePO$_4$, including carbon coating, addition of conductive copper/silver powders, dispersion of high-surface-area carbon black, supervalence cation doping and synthesis of nanosize grains [16–23].

The formation of nano-network electronic conduction in LiFePO$_4$ and LiNiPO$_4$ olivines by creating conductive iron phosphides has been reported as one efficient approach to improve the electronic conductivity [24]. However, the electrochemical performance of these olivines has not been described. Here, we show the electrochemical and magnetic properties of LiFePO$_4$ and doped Li$_{0.95}$Mg$_{0.05}$FePO$_4$ compounds.

Materials and methods

Materials synthesis

LiFePO$_4$ and Li$_{0.95}$Mg$_{0.05}$FePO$_4$ were prepared by a sol-gel preparation route. Li(OH)·H$_2$O (99.9%, Aldrich), FeC$_2$O$_4$·2H$_2$O (99%, Aldrich), NH$_4$·H$_2$PO$_4$ (97%, Aldrich) and Mg(C$_2$H$_3$O$_2$)$_2$ (99%, Aldrich) were used as reactants. The stoichiometric reactants were dissolved in deionized water, to which polyacrylic acid and citric acid were added

J. Yao · K. Konstantinov · G. X. Wang · H. K. Liu
Institute for Superconducting and Electronic Materials,
University of Wollongong,
Wollongong, NSW 2522, Australia

G. X. Wang (✉) · H. K. Liu
ARC Centre for Nanoelectromaterials,
University of Wollongong,
Wollongong, NSW 2522, Australia
e-mail: gwang@uow.edu.au
Fax: +61-2-42215731

as complexing agents for the formation of the gel. The solutions were heated and maintained at 85°C under vigorous stirring until a viscous gel was formed. The as-formed gel was heated to 500°C to decompose the organics under flowing argon gas. The decomposed precursors were further sintered at 700, 800 and 850°C, respectively, under a flowing gas mixture (10% H_2 in Ar). A slightly reducing atmosphere was employed during the sintering process to prevent the oxidation of Fe^{2+} cations. Six samples were prepared, which are listed in Table 1.

X-ray analysis and scanning electron microscopy observation

X-ray diffraction (XRD) was performed on the prepared lithium iron phosphates to determine the phase purity using Cu Kα radiation (MO3xHF22, MacScience, Japan). The morphology of lithium iron phosphate powders was studied using a scanning electron microscope (SEM; JEOL JEM-3000).

Magnetic measurements

The magnetic properties of LiFePO$_4$ and Li$_{0.95}$Mg$_{0.05}$PO$_4$ samples sintered at 700 and 850°C were studied using a Quantum Design MPMS XL SQUID magnetometer. The dc susceptibility was measured in a magnetic field of 5,000 Oe from 5 to 300 K.

Electrochemical testing

Electrochemical characterization was performed by assembling CR2032 coin cells for galvanostatic charge/discharge. The electrodes were made by dispersing 80 wt% active material, 10 wt% carbon black and 10 wt% polyvinylidene fluoride (PVDF) in n-methyl pyrrolidone (NMP) to form a slurry. The slurry was then coated onto an Al foil. The coated electrodes were dried in a vacuum oven and then pressed at 1,200 kg/cm^2. The thickness of electrodes is about 70–80 µm. The mass of active materials in each electrode is in the range of 1.5–2.0 mg. The coin cells were assembled in an argon-filled glove box (Mbraun, Unilab, Germany) with lithium foil as the counter electrode. The electrolyte was 1 M LiPF$_6$ in a 1:1 mixture of ethylene carbonate (EC) and dimethyl carbonate (DMC).

Results and discussion

XRD and SEM analyses

XRD was performed on LiFePO$_4$ and Li$_{0.95}$Mg$_{0.05}$FePO$_4$ powders. Fig. 1 shows the XRD patterns of LiFePO$_4$ and Li$_{0.95}$Mg$_{0.05}$FePO$_4$ samples sintered at different temperatures. Phase-pure LiFePO$_4$ and Li$_{0.95}$Mg$_{0.05}$FePO$_4$ were obtained after sintering at 700 and 800°C. The diffraction lines are indexed to an orthorhombic crystal structure (triphylite, space group $Pnma$). For LiFePO$_4$ sintered at 850°C, the main phase is still triphylite LiFePO$_4$, but there are substantial impurity phases such as FeP$_4$ and Fe$_2$P, as indicated in Fig. 1a. However, for Li$_{0.95}$Mg$_{0.05}$FePO$_4$ sintered at 850°C, the main phase is not triphylite. There are numerous impurity phases that cannot be totally identified. The strongest diffraction peak was identified as Fe$_2$P. XRD analysis confirmed the previous report [24] that iron phosphides are formed in LiFePO$_4$ and Li$_{0.95}$Mg$_{0.05}$FePO$_4$ compounds when sintered at high temperature. We noted that the Mg-doped sample sintered at 850°C has more impurities than that of the undoped one. This result is similar to the previous report [25] in which it was found that doped samples always contain more impurities and impurity phases were found enriched in the dopant. The mechanism for this phenomenon is unclear yet. Thermogravimetric analysis was performed on LiFePO$_4$ and Li$_{0.95}$Mg$_{0.05}$FePO$_4$ samples. All samples contain 2–3 wt% carbon, which was induced by the sol–gel synthesis process.

Fig. 2a–c shows SEM images of Li$_{0.95}$Mg$_{0.05}$PO$_4$ powders sintered at 700, 800 and 850°C, respectively. The sample sintered at 700°C has a small grain size of about 0.5–1 µm. When sintered at 800°C, the grain size increased to 3–5 µm, while the 850°C sintered sample exhibited the biggest grain size of 5–10 µm. The crystal size of lithium iron phosphates was significantly influenced by the sintering temperature. Fig. 3 shows the energy-dispersive spectrometry (EDS) elemental mapping of Li$_{0.95}$Mg$_{0.05}$PO$_4$ powders. Fig. 3a is the secondary electron image. A very uniform element distribution was observed for main elements Fe, P, and O. Due to resolution reason, the distributions of trace dopant Mg and carbon are not shown. The trace dopant Mg^{2+} ions are also observed

Table 1 Sintering temperature, label and average crystal size of lithium iron phosphates

Sample (nominal formula)	Sintering temperature (°C)	Label	Impurity phase	Average crystal size (µm)
LiFePO$_4$	700	LFP-700	NA	0.6
LiFePO$_4$	800	LFP-800	NA	4.0
LiFePO$_4$	850	LFP-850	FeP$_4$, Fe$_2$P	8.0
Li$_{0.95}$Mg$_{0.05}$FePO$_4$	700	LFPMg-700	NA	0.8
Li$_{0.95}$Mg$_{0.05}$FePO$_4$	800	LFPMg-800	NA	4.5
Li$_{0.95}$Mg$_{0.05}$FePO$_4$	850	LFPMg-850	Fe$_2$P, FeP$_4$, Fe$_2$P$_2$O$_7$ and others	10

NA Not applicable

**Fig. 1** X-ray diffraction patterns of **a** LiFePO$_4$ and **b** Li$_{0.95}$Mg$_{0.05}$FePO$_4$

a

b
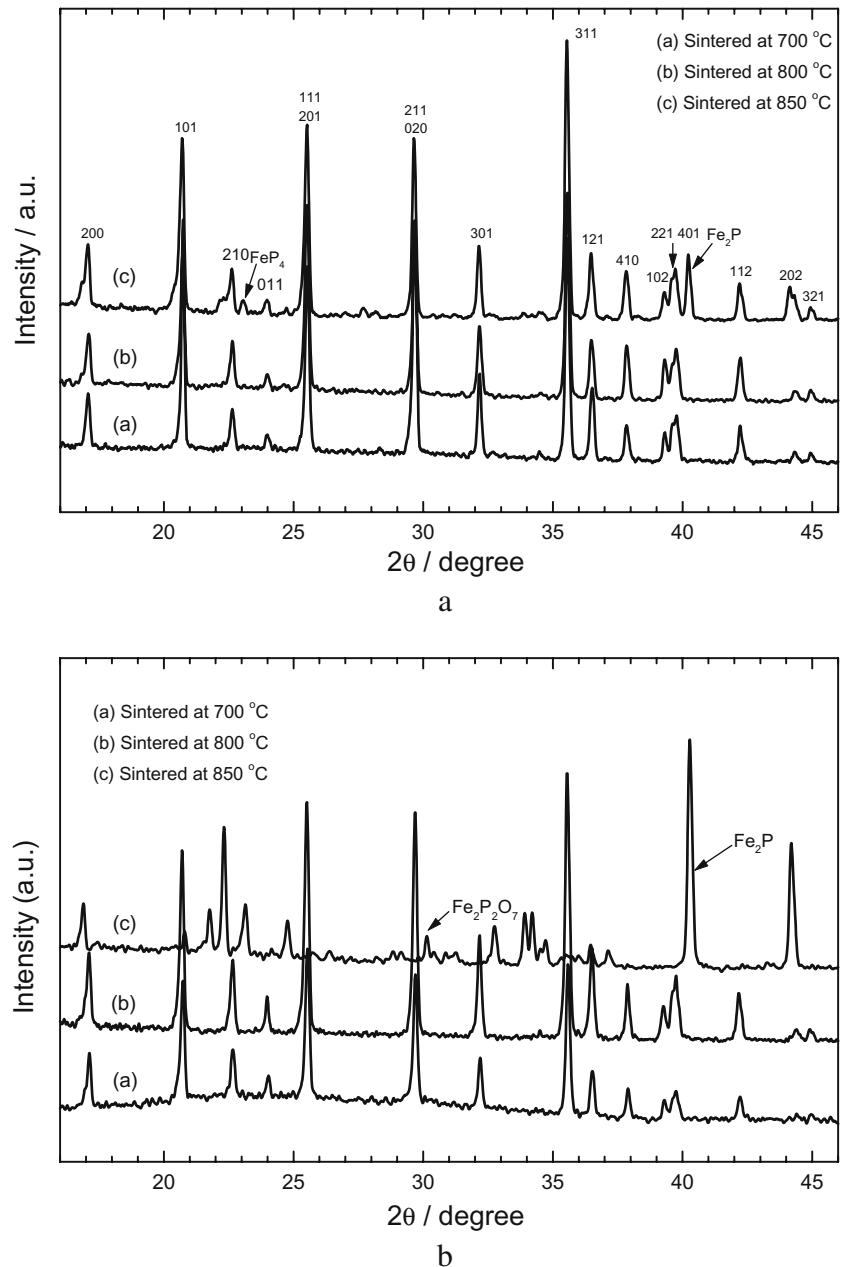
homogeneously distributed in the crystal structures. This should be attributed to the chemical synthesis process. The ingredient Li$^+$, Fe^{2+}, Mg^{2+} and PO$_4^{3-}$ ions were dissolved in water and mixed on the atomic scale in solution. Following the subsequent gel formation and sintering, a uniform element distribution in the as-prepared materials is expected. The phase compositions and average crystal size of all samples are summarized in Table 1. In general, Mg-doped samples show larger crystal size than that of undoped ones. This could be due to the promotion of crystal growth by MgO because MgO is a common assistant sintering material. We performed Rietveld refinement on XRD data for all samples to obtain lattice parameters. We found that LiFePO$_4$ and Li$_{0.95}$Mg$_{0.05}$FePO$_4$ have

the same lattice parameters within the same series, regardless of sintering temperature. LiFePO$_4$ olivine has the lattice parameters a=10.35559(7) Å, b=6.00463(4) Å and c=4.68908 (3) Å, while the Mg-doped Li$_{0.95}$Mg$_{0.05}$FePO$_4$ olivine phase has slightly small lattice parameters, a=10.3146 (1) Å, b=6.00122 (5) Å and c=4.66574 (8) Å. The unit cell of the olivine lattice was slightly shrunk along all x-, y- and z-directions due to the doping effect. This is in agreement with the fact that Mg^{2+} ion (r=0.66 Å) has smaller radius than that of Fe^{2+} ion (r=0.74 Å) in octahedral coordination. The variation of lattice parameters further confirms the incorporation of Mg^{2+} ions in olivine crystal structure.

Fig. 2 Scanning electron microscopy (SEM) images of $Li_{0.95}Mg_{0.05}FePO_4$ samples sintered at **a** 700°C, **b** 800°C and **c** 850°C
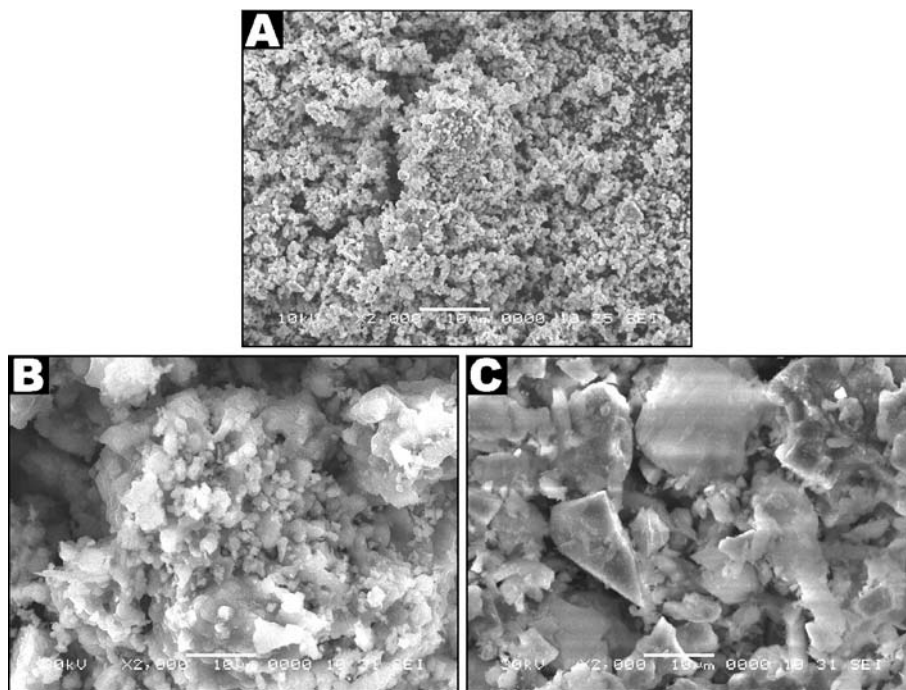
Magnetic properties of $LiFePO_4$ and $Li_{0.95}Mg_{0.05}FePO_4$

The temperature dependencies of the molar magnetic susceptibilities of $LiFePO_4$ samples sintered at 700 and 850°C are shown in Fig. 4a,b respectively. The reciprocal susceptibilities are shown in the inset. The magnetic susceptibility of $LiFePO_4$ shows a maximum at 50±2 K, demonstrating a paramagnetic–antiferromagnetic phase transition with a Curie–Weiss behaviour above the Néel temperature (θ_N). The two samples show similar dependencies of the magnetic susceptibilities on temperature, but the sample sintered at 850°C shows lower molar susceptibility. As detected by XRD analysis, a small amount of

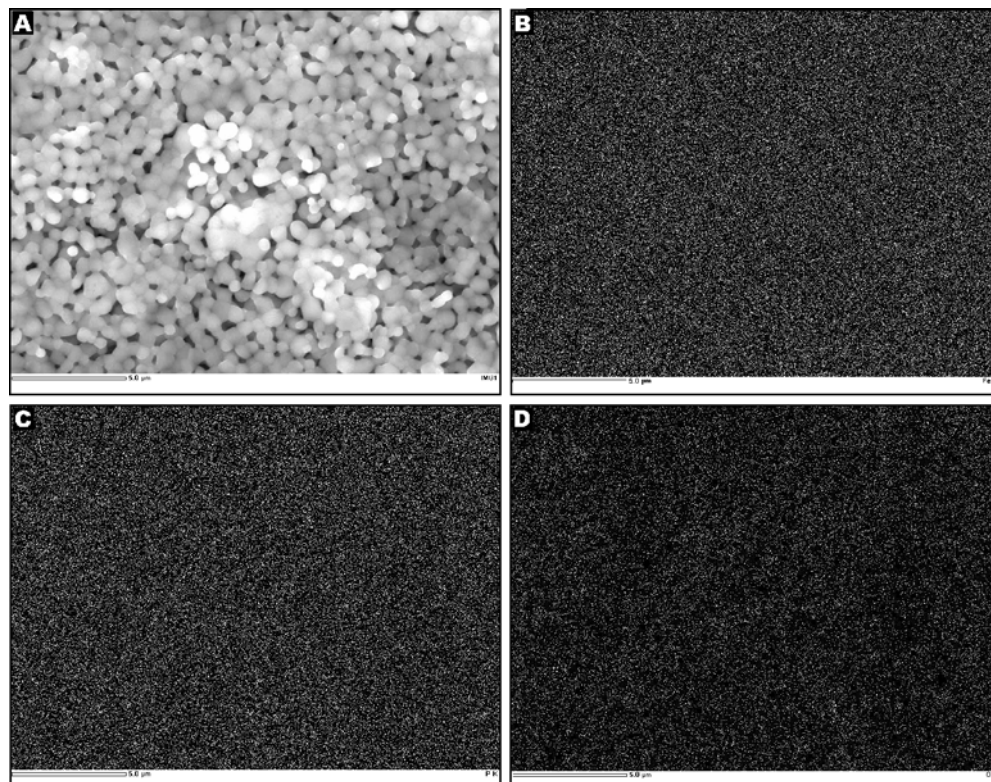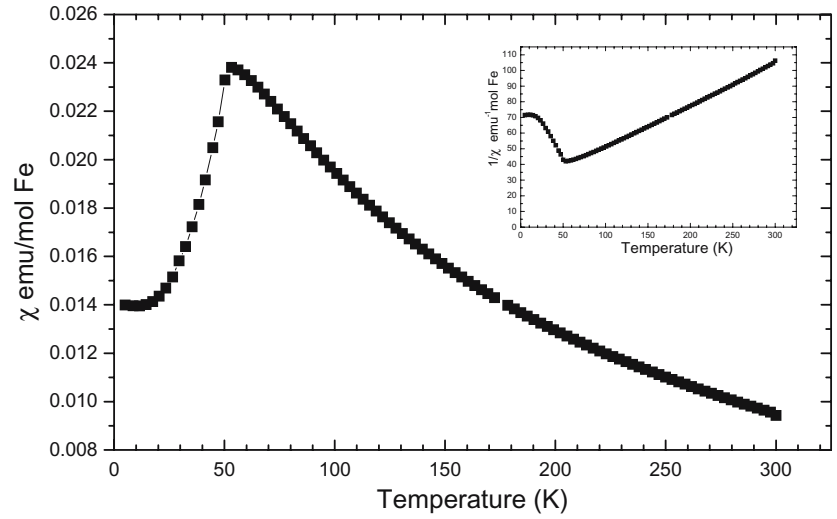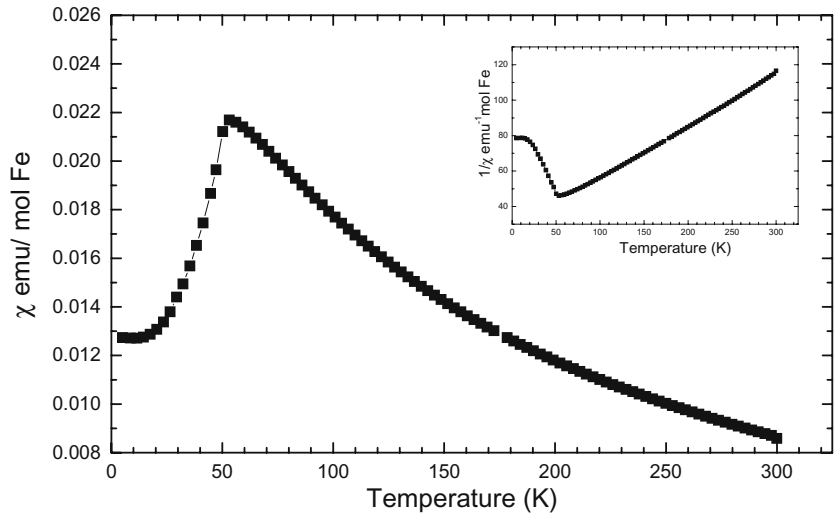**Fig. 3** Energy-dispersive spectrometry (EDS) elemental mapping by SEM

Fig. 4 Temperature dependencies of molar magnetic susceptibilities of LiFePO$_4$ samples. **a** LFP-700. **b** LFP-850. The *insets* are reciprocal magnetic susceptibilities


iron phosphides in LiFePO$_4$ was formed when sintered at 850°C, but this has no significant influence on the antiferromagnetic behaviour. Fig. 5a,b shows the molar magnetic susceptibilities of Li$_{0.95}$Mg$_{0.05}$FePO$_4$ powders sintered at 700 and 850°C, respectively. The Li$_{0.95}$Mg$_{0.05}$FePO$_4$ sample sintered at 700°C shows the same magnetic behaviour as LiFePO$_4$, with a typical antiferromagnetism below the Néel temperature. However, the Li$_{0.95}$Mg$_{0.05}$FePO$_4$ sample sintered at 850°C shows ferromagnetic behaviour, which is totally different from its counterpart sintered at 700°C. The main phases for Li$_{0.95}$Mg$_{0.05}$FePO$_4$ sintered at 850°C are iron phosphides. Most of these phosphides (Fe$_2$P, Fe$_3$P, FeP$_4$ and Fe$_{75}$P$_{15}$C$_4$) are ferromagnetic [26]. Therefore, the measured ferromagnetic behaviour also confirmed the formation of substantial ferromagnetic iron phosphides when sintered at high temperature (850°C).

The effective magnetic moment was obtained using the paramagnetic formula $\mu=(8\chi T)^{-1/2}$ [27] by using measured magnetic susceptibility, which is shown in Fig. 6. The measured μ values for the three antiferromagnetic samples are in the range of 4.6–4.9 μ_B at room temperature. The Curie temperature θ_C was obtained by linear fitting the reciprocal magnetic susceptibility above the Néel temperature. Table 2 shows the magnetic parameters of the four samples. All three antiferromagnetic samples have the same Néel temperature. The Mg-doped sample sintered at 700°C shows a different Curie temperature of $\theta_C=-76$ K. The ferromagnetic sample has a positive θ_C value of 110.5 K.

In the triphylite structure of LiFePO$_4$, Fe^{2+} ions occupy octahedral 4c sites with coordinates $x=0.28$, $y=0.25$ and $z=0.96$. Due to the influence of the octahedral crystal field, the five 3d orbitals of the Fe^{2+} ion split into three t$_{2g}$ and two e$_g$ configurations. There are six electrons in 3d orbitals for the Fe^{2+} ion. Among them, four electrons are on the three t$_{2g}$ orbitals (d_{xy}, d_{xz} and d_{yz}), in which three electrons spin up and the fourth electron spins down. The magnetic moments for the paired two electrons in one of the t$_{2g}$ orbitals cancel each other. Therefore, there is a net of two

Fig. 5 Temperature dependencies of molar magnetic susceptibilities of $Li_{0.95}Mg_{0.05}FePO_4$ samples. **a** LFPMg-700. **b** LFPMg-850. The *insets* are reciprocal magnetic susceptibilities
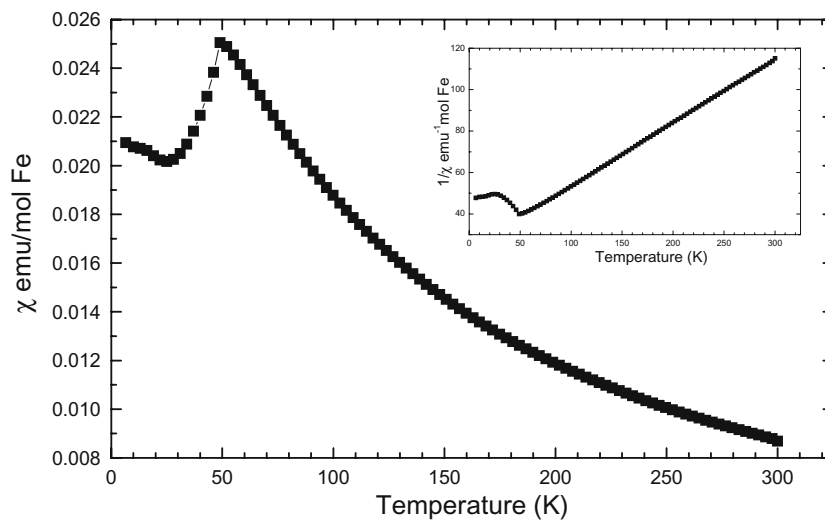
a
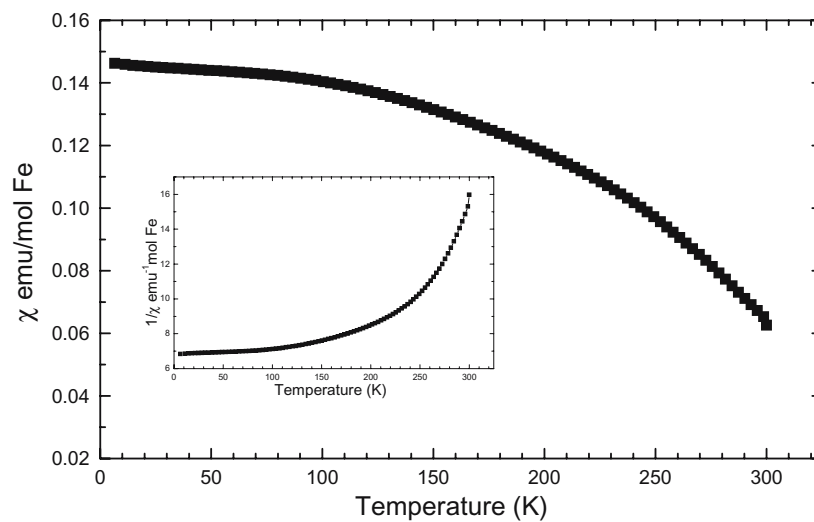
b

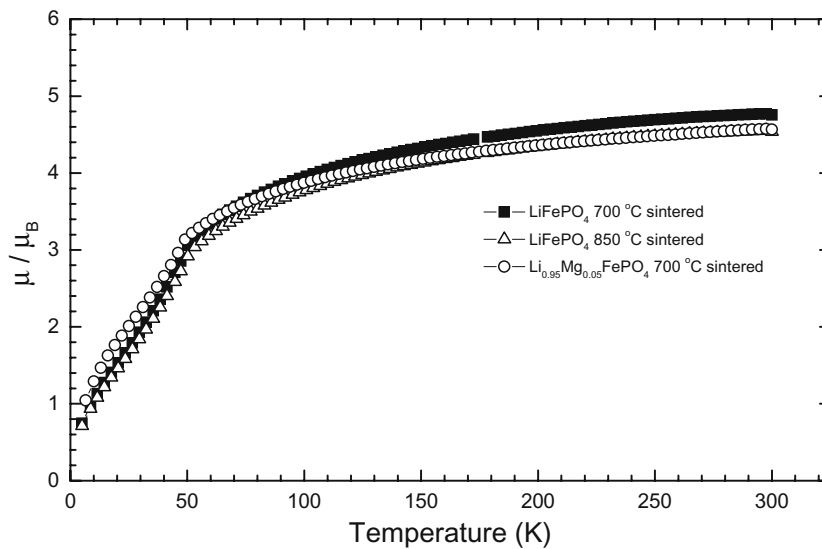**Fig. 6** The effective magnetic moment per mole of iron of $LiFePO_4$ and $Li_{0.95}Mg_{0.05}FePO_4$ samples

Table 2 Magnetic parameters of LiFePO₄ and doped Li₀.₉₅Mg₀.₀₅FePO₄ samples

Sample	Magnetic properties		
	Néel temperature, T_N (K)	Curie temperature, θ_C (K)	Effective magnetic moment, μ (μ_B) at 25°C
LiFePO₄, 700°C sintered	50±2	−96.2	4.77
LiFePO₄, 850°C sintered	50±2	−96.2	4.55
Li₀.₉₅Mg₀.₀₅FePO₄, 700°C sintered	50±2	−76.0	4.57
Li₀.₉₅Mg₀.₀₅FePO₄, 850°C sintered	–	+110.5	

spin-up electrons in t_{2g} orbitals. Two electrons occupy two e_g orbitals (d_{x2-y2} and $d_z{}^2$), in which one electron is in each orbital with spin-up configuration. The Fe^{2+} ion presents a net of four spin-up electrons (high spin). Therefore, the theoretical value of magnetic moment μ for Fe^{2+} in LiFe PO₄ would be 4.90 μ_B based on the formula $\mu = g[S(S+1)]^{1/2}$, where $g = 2.0023$ and $S = 2$. Our experimental value agrees quite good with the theoretical value. Following the super and super–super exchange rule, the interactions between Fe–O–Fe induce antiferromagnetism, as exhibited by the magnetic measurement. However, in the orthorhombic phase, there is no Fe–O–Fe bonding, only Fe–O–P–O–Fe bonding. Thus, the magnetic interaction in LiFePO₄ could be long range through Fe–O–P–O–Fe triple exchange [28–30].

Fig. 7 Charge/discharge curves in the first cycle for **a** LiFePO₄ and **b** Li₀.₉₅Mg₀.₀₅FePO₄ sample electrodes. Current rate: $C/8$
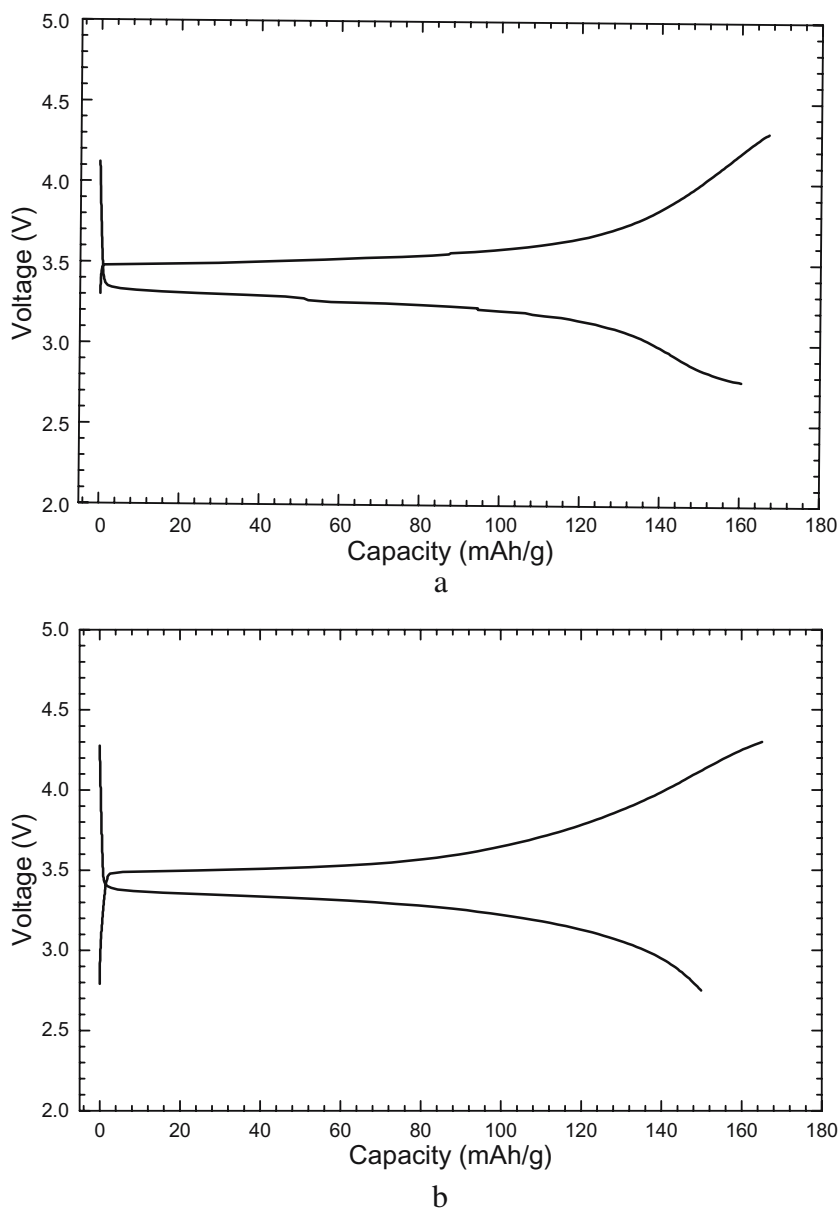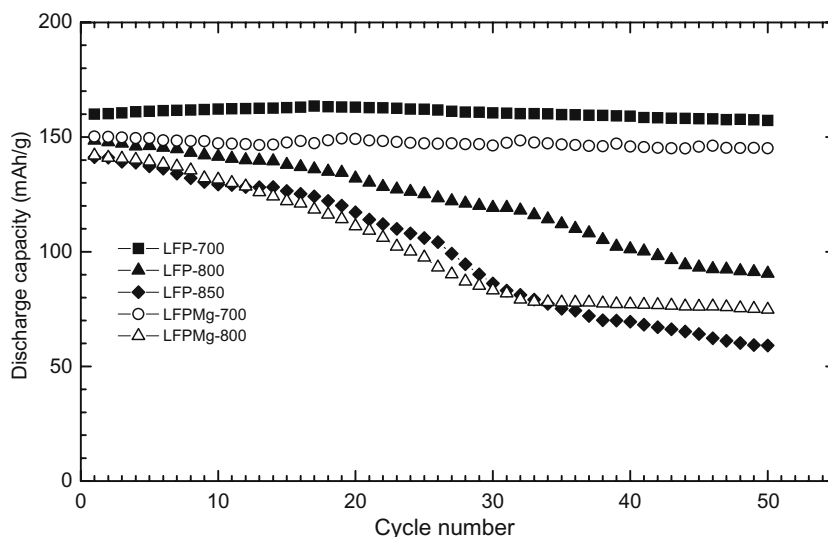
Fig. 8 Discharge capacity vs
cycle number for LiFePO$_4$ and
Li$_{0.95}$Mg$_{0.05}$FePO$_4$ sample elec-
trodes. Current rate: $C/8$

Electrochemical performance of LiFePO$_4$
and Li$_{0.95}$Mg$_{0.05}$FePO$_4$ cathode materials

Electrochemical properties of LiFePO$_4$ and Li$_{0.95}$Mg$_{0.05}$PO$_4$
cathodes were characterized via constant current charge/
discharge testing at $C/8$ rate. Fig. 7a,b shows the voltage
profiles in the first cycle for LFP-700 and LFPMg-700
sample electrodes. The cells were charged and discharged
in the voltage range of 2.75–4.2 V vs Li/Li$^+$. The profiles
exhibit a flat charge and discharge plateau between 3.45
and 3.55 V, which matches the oxidation and reduction
peaks in the $C–V$ curves. LiFePO$_4$ electrode delivered a
specific discharge capacity of 160 mA h/g in the first cycle,
whereas Li$_{0.95}$Mg$_{0.05}$FePO$_4$ cathode shows a lower dis-
charge capacity of 150 mA h/g in the first cycle, which is
due to the partial substitution of Li$^+$ with non-active Mg^{2+}.
The cyclabilities of all sample electrodes are shown in
Fig. 8. In general, the as-prepared LiFePO$_4$ and Li$_{0.95}$
Mg$_{0.05}$FePO$_4$ cathode materials sintered at different
temperatures demonstrated a stable capacity in the range
of 150–160 mA h/g at the $C/8$ rate. The capacity
degradation with cycling for LiFePO$_4$ and Li$_{0.95}$Mg$_{0.05}$
FePO$_4$ sample electrodes increases with increasing sinter-
ing temperature, which is due to the influence of the
increased crystal size. The previously proposed "radial
model" and "mosaic model" for LiFePO$_4$ can exactly
explain the observed phenomena [31, 32]. The process of
lithium insertion and extraction on LiFePO$_4$ is a two-phase
coexisting process. Therefore, the crystal size has a critical
influence on the transport of lithium ions and electrons into
and out of the individual crystal. The larger the crystal size,
the greater the inefficiency of the full conversion of
LiFePO$_4$ to FePO$_4$ and back again, inducing a loss of
capacity with cycling.

Conclusions

The sintering temperature has significant influences on the
crystal size and impurities of LiFePO$_4$ and Li$_{0.95}$Mg$_{0.05}$FePO$_4$

compounds. Substantial iron phosphides can be formed
when sintered at high temperatures. Typical antiferromag-
netic behaviour was demonstrated for LiFePO$_4$ and
Li$_{0.95}$Mg$_{0.05}$FePO$_4$ samples with a Néel temperature (T_N)
of 50±2 K. This antiferromagnetism could be induced by
long-range Fe–O–P–O–Fe triple exchange. LiFePO$_4$ and
Li$_{0.95}$Mg$_{0.05}$FePO$_4$ compounds are electrochemically ac-
tive, with a specific capacity between 150 and 160 mA h/g.

References

1. Tarascon JM, Armand M (2001) Nature 414:359
2. Walkihara M (2001) Mater Sci Eng R 33:109
3. Tirado JL (2003) Mater Sci Eng R 40:103
4. Whittingham MS (2004) Chem Rev 104:4271
5. Armstrong AR, Bruce PG (1996) Nature 381:499
6. Ammundsen B, Desilvestro J, Groutso T, Hassell D, Metson
   JB, Regan E, Steiner R, Pickering PJ (2000) J Electrochem Soc
   147:4078
7. Thackeray MM (1995) J Electrochem Soc 142:2558
8. Li GH, Ikuta H, Uchida T, Wakihara M (1996) J Electrochem
   Soc 143:178
9. Saadoune I, Delmas C (1996) J Mater Chem 6:193
10. Armstrong AR, Paterson AJ, Robertson AD, Bruce PG (2002)
    Chem Mater 14:710
11. Padhi AK, Nanjundaswamy KS, Goodenough JB (1997) J
    Electrochem Soc 144:1188
12. Padhi AK, Nanjundaswamy KS, Masquelier C, Goodenough
    JB (1997) J Electrochem Soc 144:1609
13. Amine K, Yasuda H, Yamachi M (2000) Electrochem Solid
    State Lett 3:178
14. Huang H, Yin SC, Kerr T, Taylor N, Nazar LF (2002) Adv
    Mater 14:1525
15. Delacourt C, Poizot P, Morcrette M, Tarascon JM, Masquelier
    C (2004) Chem Mater 16:93

16. Huang H, Yin SC, Nazar LF (2001) Electrochem Solid State Lett 4:A170
17. Yamada A, Chung SC, Hinokuma K (2001) J Electrochem Soc 148:A224
18. Croce F, D'Epifanio A, Hassoun J, Deptula A, Olczac T, Scrosati B (2002) Electrochem Solid State Lett 5:A47
19. Franger S, Cras FL, Bourbon C, Rouault H (2002) Electrochem Solid State Lett 5:A231
20. Barker J, Saidi MY, Swoyer JL (2003) Electrochem Solid State Lett 6:A53
21. Wang GX, Bewlay S, Yao J, Ahn JH, Dou SX, Liu HK (2004) Electrochem Solid State Lett 7:A503
22. Franger S, Bourbon C, Cras FL (2004) J Electrochem Soc 151: A1024
23. Mi CH, Zhao XB, Cao GS, Tu JP (2005) J Electrochem Soc 152:A483
24. Herle PS, Ellis B, Coombs N, Nazar LF (2004) Nat Mater 3:147
25. Chung SY, Blocking JT, Chiang YM (2002) Nat Mater 1:123
26. Berry BS, Pritchet WC (1978) Solid State Commun 26:827
27. Song YN, Zavalij PY, Chernova NA, Whittingham MS (2005) Chem Mater 17:1139
28. Santoro RP, Newnham RE (1967) Acta Crystallogr 22:344
29. Song YN, Zavalij PY, Suzuki M, Whittingham MS (2002) Inorg Chem 41:5778
30. Rousse G, Rodriguez-Carvajal J, Patoux S, Masquelier C (2003) Chem Mater 15:4082
31. Andersson AS, Kalska B, Häggström L, Thomas JO (2000) Solid State Ionics 130:41
32. Andersson AS, Thomas JO (2001) J Power Sources 97–98:498